Supplementary Information (SI) for Inorganic Chemistry Frontiers.

Supporting Information

Pore-Structure Control in Bimetallic Coordination Networks for Natural Gas Purification with Record C_2H_6/CH_4 Selectivity

Li-Ping Zhang, [a] *Yi-Tao Li,* [a] *Yu Jiang,* [a] *Run-Yuan Jiang,* [a] *Shuang Ni,* [a] *Qing-Yuan Yang**[a]

[a] School of Chemical Engineering and Technology, Xi’an Jiaotong University, Xi’an 710049, China.

E-mail: qingyuan.yang@xjtu.edu.cn

CONTENTS

1. Experimental Section

Materials: Indium nitrate hydrate ($In(NO_3)_3 \cdot xH_2O$, 99.99%) and cuprous iodide (CuI, ≥99.5%) were purchased from Shanghai Aladdin Bio-Chem Technology Co., Ltd. isonicotinic acid (99.96%) and 3-aminoisonicotinic acid (97%) were purchased from Shanghai Bide Pharmaceutical Technology Co., Ltd. N,N-dimethylformamide (DMF, ≥99.5%) was purchased from Sinopharm Chemical Reagent Co.,Ltd. Methanol (CH_3OH, 99.5%) was purchased from shanghai McLean Biochemical Technology Co., Ltd. All reagents and solvents received were used without further purification.

Synthesis of ***CuIn(ina)***$_4$*:* The $CuIn(ina)_4$ was synthesized according to the literature method.[1] CuI (95 mg, 0.5 mmol), $In(NO_3)_3 \cdot xH_2O$ (150 mg, 0.5 mmol), isonicotinic acid (246 mg, 2 mmol), 4.5 mL DMF and 0.5 mL methanol were mixed in a heat-resistant glass bottle. In an oven, the mixture was heated under 100°C for 3 days to produce red crystal. The as-synthesized $CuIn(ina)_4$ was soaked in acetonitrile (CH_3CN) for one week, during which CH_3CN was replaced per day. The activated sample for gas adsorption can be obtained by heating at 100°C for 12 h under vacuum condition.

Synthesis of ***CuIn(3-ain)***$_4$*:* The $CuIn(3\text{-}ain)_4$ powder was synthesized according to the literature method.[2] CuI (95 mg, 0.5 mmol), $In(NO_3)_3 \cdot xH_2O$ (150 mg, 0.5 mmol), 3-aminoisonicotinic acid (276 mg, 2 mmol), 4.5 mL DMF and 0.5 mL methanol were mixed in a heat-resistant glass bottle. The reaction and activation conditions were the same as for $CuIn(ina)_4$. (Yield: 303.5 mg, 83.52%).

Characterization: X-ray diffraction (XRD) was carried out using the XRD-6100 diffractometer equipped with a Cu tube. The products were recorded in the 2θ range from 6.0° to 50.0°. Thermogravimetric analysis (TGA) were carried out using a

NETZSCH STA449F5 instrument under a nitrogen atmosphere (nitrogen flow rate of 50 mL min^{-1}). Sample was heated in closed alumina cells at a heating rate of 10 °C min^{-1} in the temperature in the range of 25-700 °C. Fourier transform infrared spectroscopy (FT-IR) spectra were obtained by using Nicolet iS50 FT-IR spectrometer.

Single-Component Gas Adsorption Measurements: Before sorption analysis, all the samples were activated under a vacuum condition. The single-component adsorption isotherms of CO_2 were performed on BSD-PMC (Beishide Instrument) at 195 K. The single-component adsorption isotherms of CH_4, C_2H_6 and C_3H_8 were performed on JW-BK200C (JWGB Sci & Tech Co. Ltd.) at different temperatures (273 K, 298 K, and 313 K for CH_4, C_2H_6 and C_3H_8). The temperatures during sorption measurements were precisely maintained using anhydrous ethanol as a constant temperature bath. Temperatures of 195 K was achieved with isopropyl alcohol-dry ice bath.

Adsorption rate curves: CH_4, C_2H_6 and C_3H_8 gases were introduced into the MOF material within the sample tube at 298 K and a pressure of 100 kPa, respectively. The instantaneous adsorption rates of CuIn(ina)$_4$ and CuIn(3-ain)$_4$ on the three gases could be calculated by recording the capacity of adsorbed gases at each moment of time by the MOF materials.

Calculation of gas occupancy and gas density: Gas occupancy for CH_4, C_2H_6, and C_3H_8 in CuIn(ina)$_4$ and CuIn(3-ain)$_4$ were calculated by the following equation:

$$Gas\ occupancy = Q * NA * \rho * V_c * 10^{-27}$$

Here, Q (mmol g^{-1}) is the saturated gas uptake; NA is the Avogadro constant; ρ (g cm^{-3}) is the structure density and V_c ($Å^3$) is the cell volume. Calculated results are shown in Table S2.

Gas density of CH_4, C_2H_6, and C_3H_8 in the pore of CuIn(ina)$_4$ and CuIn(3-ain)$_4$ were calculated by the following equation:

$$Gas\ density = Q * 10^{-3} * M/V_p$$

Here, Q (mmol g^{-1}) is the saturated gas uptake; M is the molar mass (g mol^{-1}) and V_p (ml g^{-1}) is the pore volume. The calculated results are shown in Table S3.

Breakthrough experiments: Breakthrough measurements were performed using BSD-MAB Analyzer coupled with a gas BSD-mass mass spectrometry (TCD-Thermal Conductivity Detector, detection limit 1 ppm) from Beishide Co, Ltd. Before breakthrough experiment, MOF powder samples were packed into a glass penetration column with an internal diameter of 5 mm and then purged with He flow (20 mL min^{-1}) at least 2 h at 100°C. Subsequently, the glass column was placed in a circulating water bath to control the reaction temperature, and then the $CH_4/C_2H_6/C_3H_8$ gas mixture ($CH_4/C_2H_6/C_3H_8$, v/v/v=85/10/5, total flow rate of 8 mL min^{-1}) was introduced into the system. Meanwhile, passed gas signals were detected by mass spectrometry in real time.

The CH_4 productivity (*q*) is defined by the breakthrough amount of CH_4 (defined as a volume of gas at STP) from an adsorption bed packed with 1 kg of MOF. The breakthrough amount was calculated by integration of the breakthrough curves during a period from t_1 to t_2 during which the CH_4 purity is higher than or equal to to a threshold value p (such as 99.9999%):

$$q = \frac{\int_{t_1}^{t_2} F_{CH_4,out} dt}{m_{MOF}}$$

Where $F_{CH_4,out}$ the flowrate of effluent CH_4 and m_{MOF} is the amount of MOF packed in the bed.

2. IAST selectivity calculation details

Before calculating IAST selectivity, the single-component gas adsorption isotherms were fit using a dual-site Langmuir-Freundlich equation, which is

$$q = \frac{A1 \times B1 \times P^{C1}}{1 + B1 \times P^{C1}} + \frac{A2 \times B2 \times P^{C2}}{1 + B2 \times P^{C2}}$$

where q is the quantity of gases adsorbed in mmol g^{-1}, A is the amount adsorbed when saturated with the gas in mmol g^{-1}, B is the Langmuir parameter in kPa^{-1}, P is gas pressure in kPa, C is the dimensionless Freundlich parameter, and subscripts 1 and 2 correspond to two different site identities.

Adsorption selectivity of C_3H_8/CH_4 or C_2H_6/CH_4, mixed gases were predicted from single component adsorption isotherms using Ideal Adsorbed Solution Theory (IAST).

$$S_{ads=} \frac{X_1/X_2}{Y_1/Y_2}$$

Where S is the selectivity of component 1 relative to 2. X_1 and X_2 are the molar fractions of components 1 and 2 in the adsorption phase, respectively. Y_1 and Y_2 are molar fractions of components 1 and 2 in the gas phase, respectively.

3. Adsorption enthalpy calculation details

Using data from 273 and 298 K, the adsorption enthalpy was calculated fitting by the Virial equation. P is the pressure described in Pa, N is the adsorbed amount in mmol/g, T is the temperature in K, a_i and b_i are Virial coefficients, and m and n are the number of coefficients used to describe the isotherms. ***Q_{st}*** is the coverage-dependent enthalpy of adsorption and R is the universal gas constant.

$$LnP = LnN + \sum_{i=0}^{m} a_i N^i + \sum_{i=0}^{n} \binom{n}{k} b_i N^i$$

$$Q_{st} = -R \sum_{i=0}^{m} a_i N^i$$

4. Theoretical studies

The computational part of the work was carried out at Shanxi Supercomputing Center of China, and the calculations were performed on TianHe-2. The host-guest interactions were calculated using Material Studio software package. Before the Grand Canonical Monte Carlo (GCMC) simulations, the guest molecules CH_4, C_2H_6, and C_3H_8 were geometrically optimized using Forcite code.[3] The Metropolis method [4] was applied to perform the GCMC simulations. The standard Universal force field described the guest-framework interactions. For each state point, the system was equilibrated for 1×10^6 steps, and then the ultimate data were collected for another 1×10^7 steps. The locate task simulated the beneficial adsorption sites with a single guest molecule.

5. Tables and figures

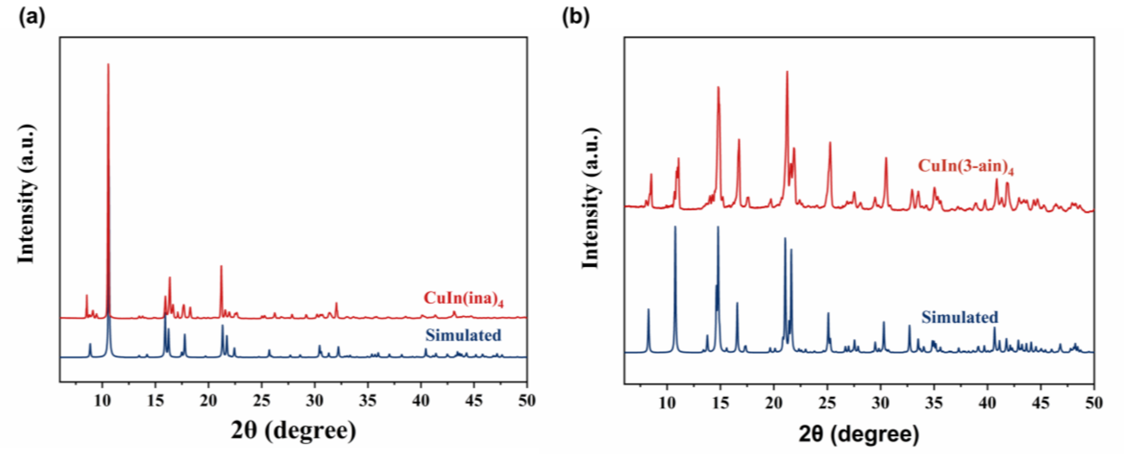

Figure S1. PXRD patterns of (a) CuIn(ina)$_4$ and (b) CuIn(3-ain)$_4$.

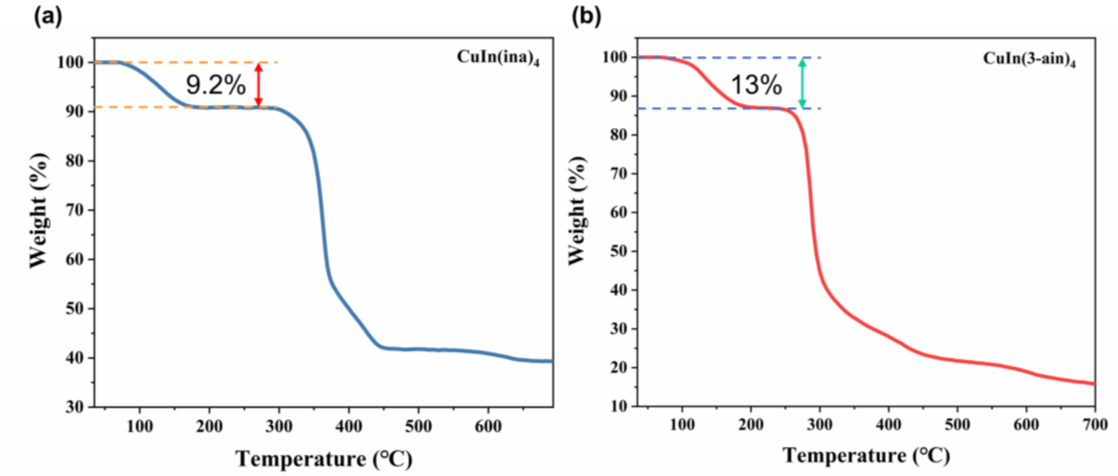

Figure S2. TGA analysis curve of (a) $CuIn(ina)_4$ and (b) $CuIn(3\text{-}ain)_4$. The data were collected under 10 K min^{-1} of heating rate.

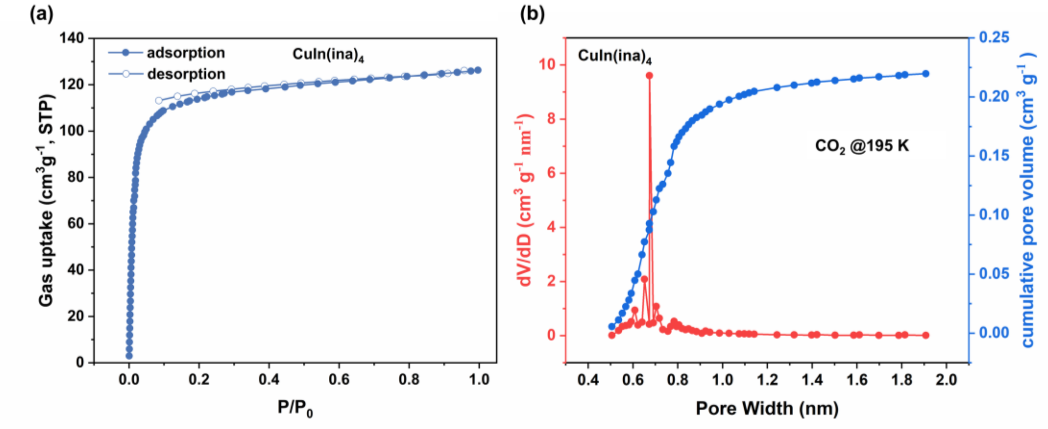

Figure S3. (a) CO_2 adsorption and desorption isotherms at 195 K for CuIn(ina)$_4$. (b) Pore size distribution for CuIn(ina)$_4$ analyzed by HK method.

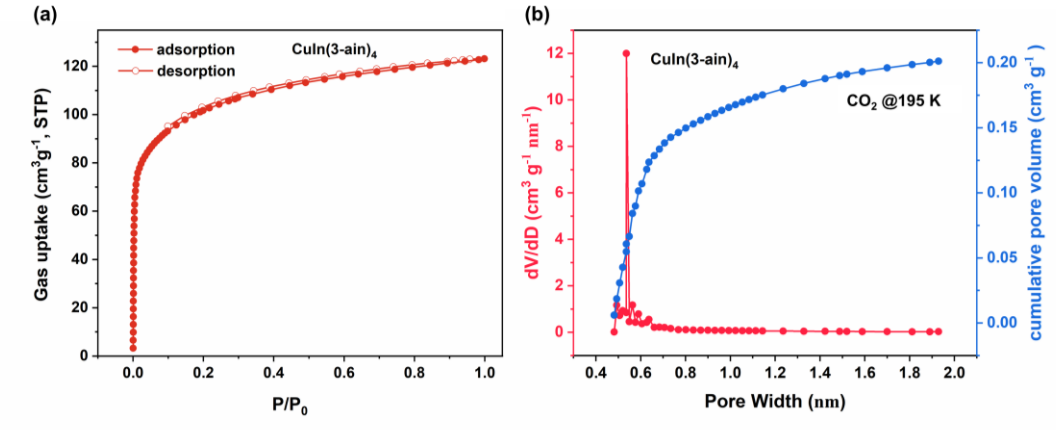

Figure S4. (a) CO_2 adsorption and desorption isotherms at 195 K for $CuIn(3\text{-}ain)_4$. (b) Pore size distribution for $CuIn(3\text{-}ain)_4$ analyzed by HK method.

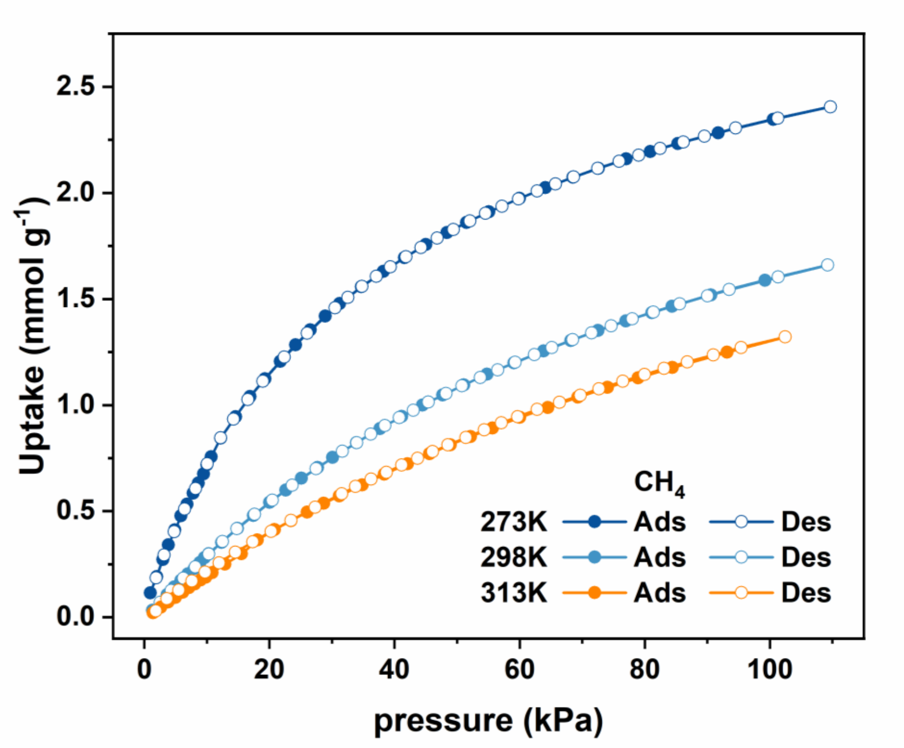

Figure S5. Adsorption isotherms of CH_4 on $CuIn(ina)_4$ at 273 K, 298 K, and 313 K.

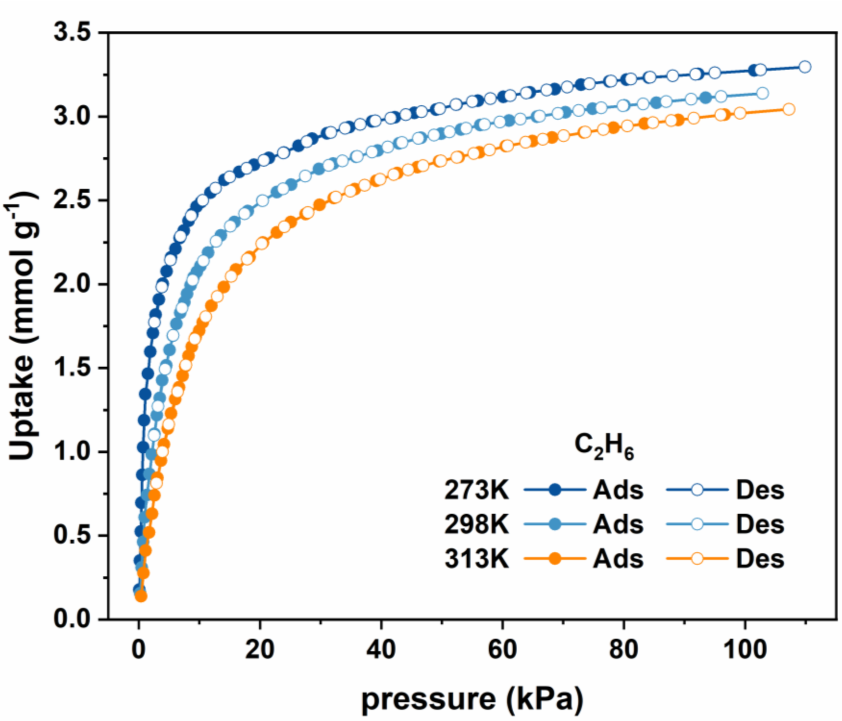

Figure S6. Adsorption isotherms of C_2H_6 on CuIn(ina)$_4$ at 273 K, 298 K, and 313 K.

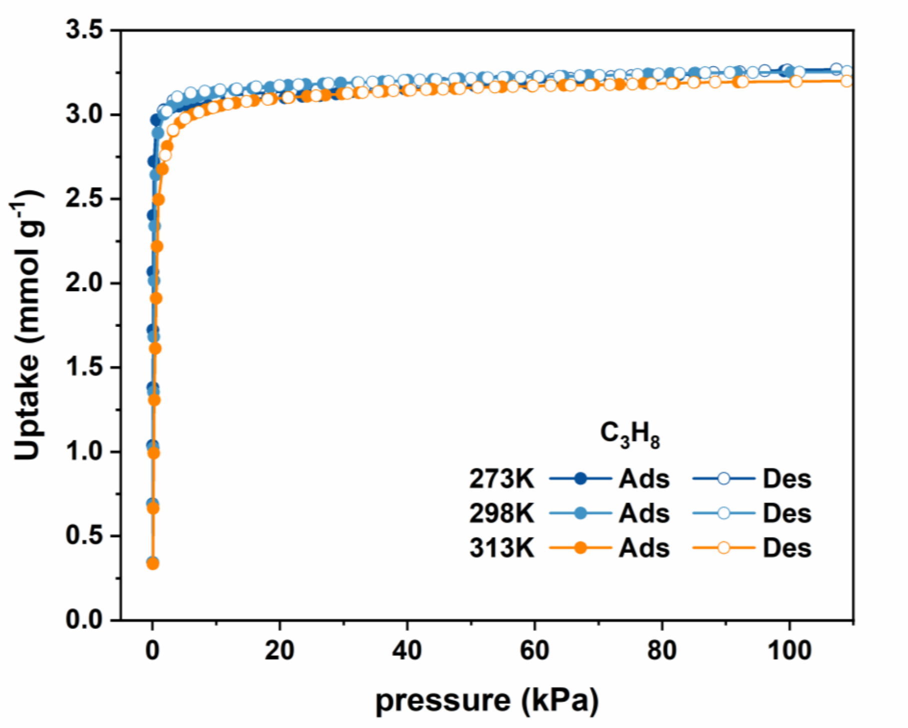

Figure S7. Adsorption isotherms of C_3H_8 on CuIn(ina)$_4$ at 273 K, 298 K, and 313 K.

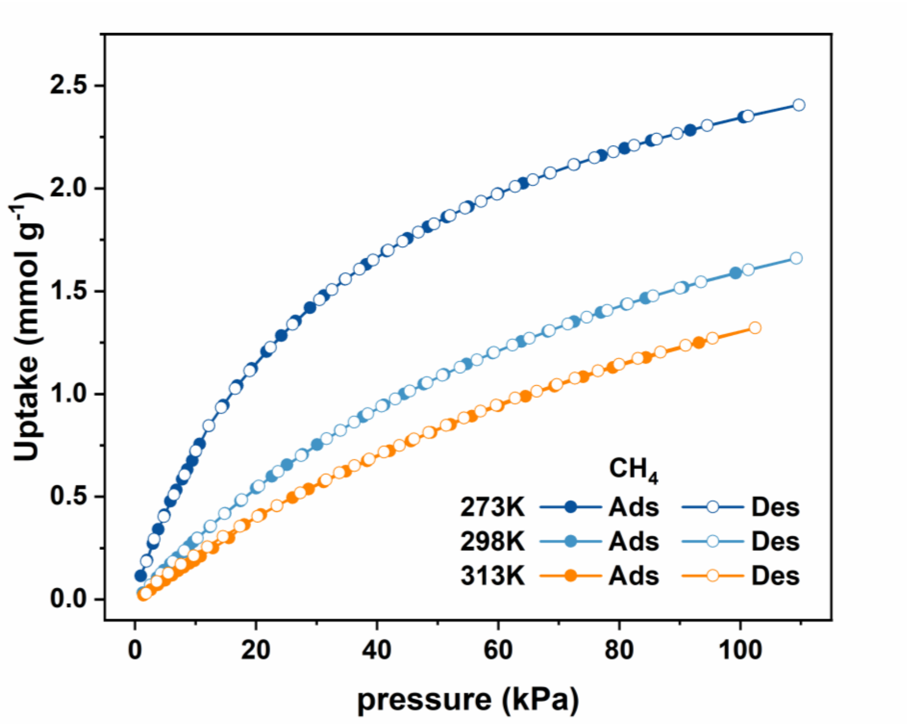

Figure S8. Adsorption isotherms of CH_4 on CuIn(3-ain)$_4$ at 273 K, 298 K, and 313 K.

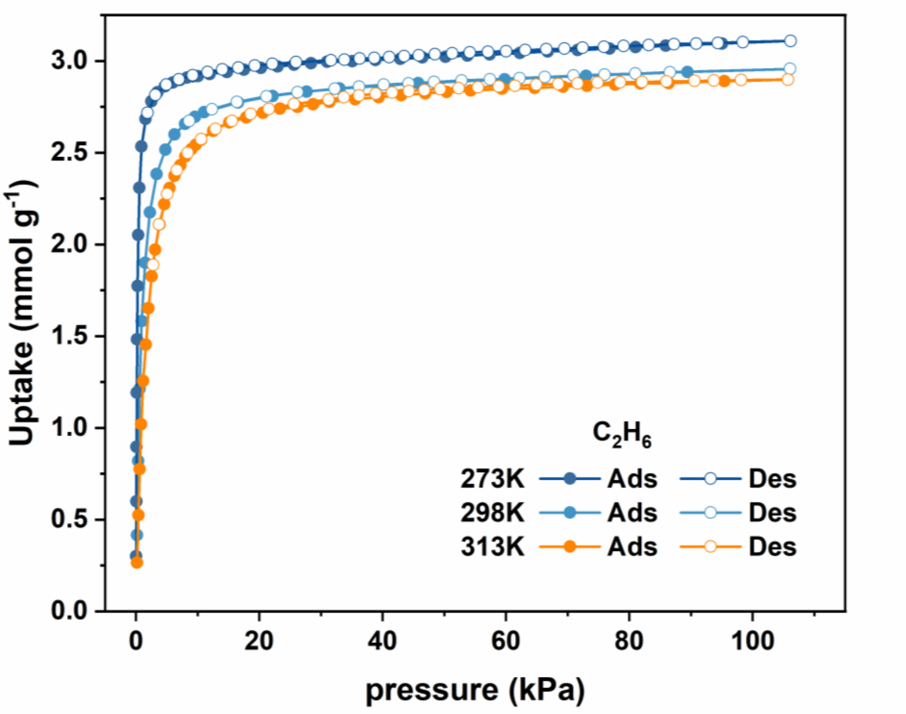

Figure S9. Adsorption isotherms of C_2H_6 on CuIn(3-ain)$_4$ at 273 K, 298 K, and 313 K.

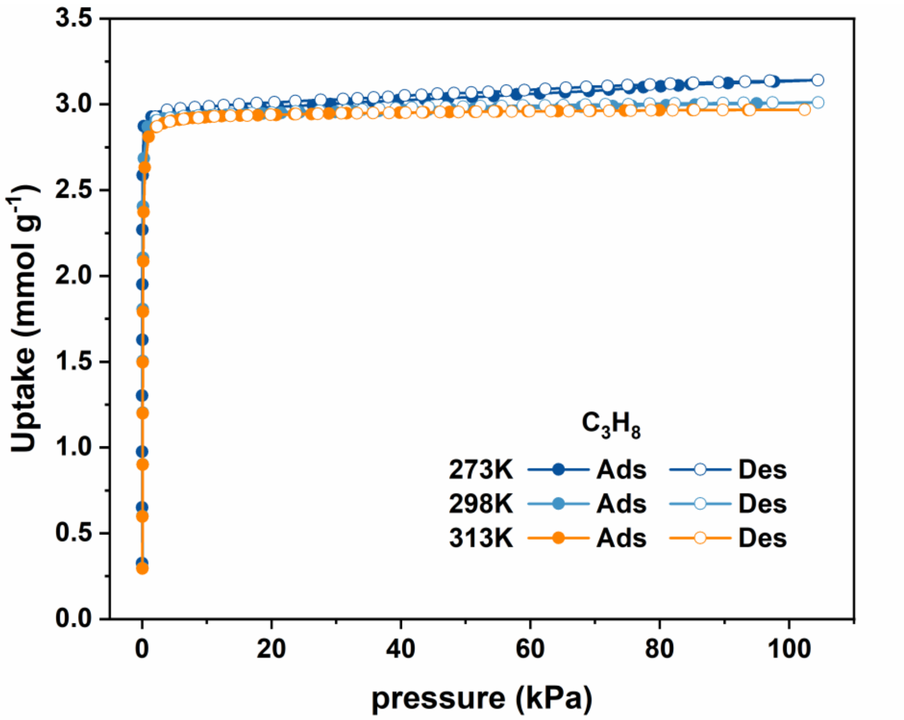

Figure S10. Adsorption isotherms of C_3H_8 on CuIn(3-ain)$_4$ at 273 K, 298 K, and 313 K.

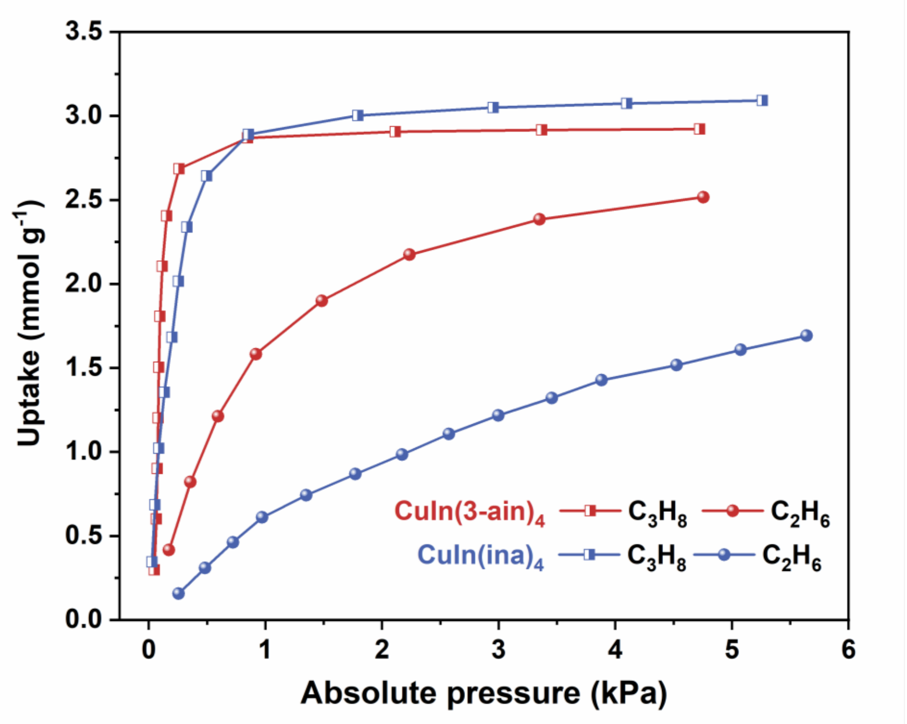

Figure S11. Comparison of C_2H_6 and C_3H_8 uptake (0-5 kPa) between CuIn(3-ain)$_4$ and CuIn(ina)$_4$.

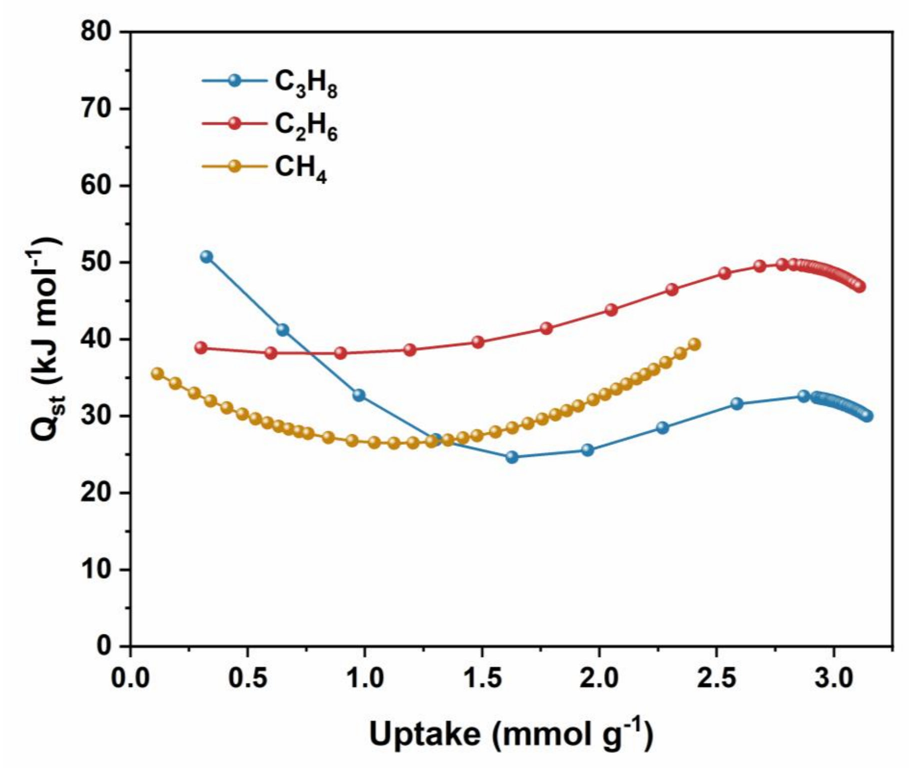

Figure S12. Q_{st} of CH_4, C_2H_6, and C_3H_8 adsorption in CuIn(3-ain)$_4$.

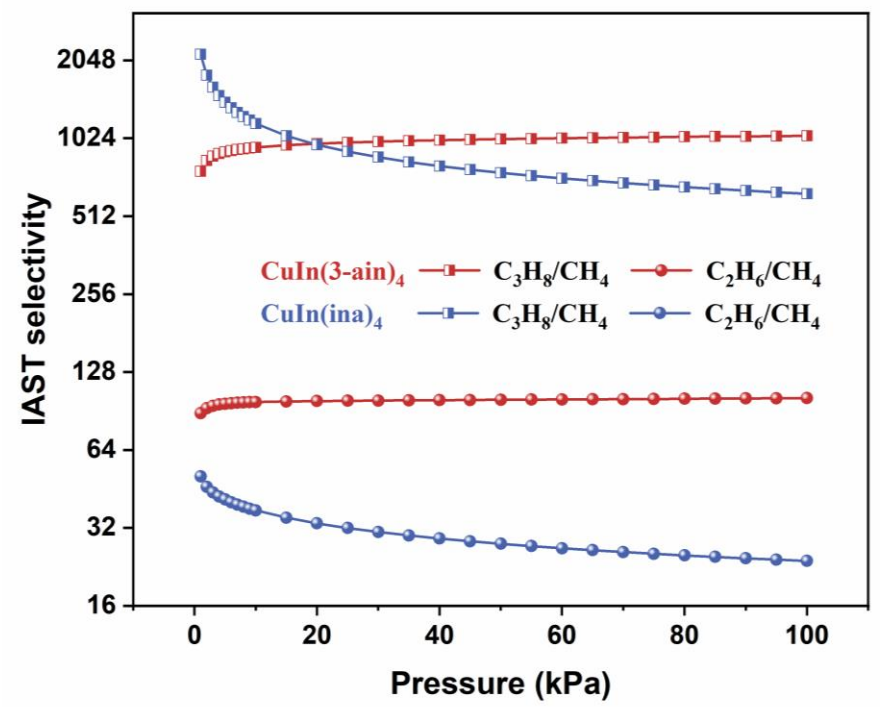

Figure S13. IAST selectivity of CuIn(ina)$_4$ and CuIn(3-ain)$_4$ towards C_3H_8/CH_4 (50:50) and C_2H_6/CH_4 (50:50) at 298 K.

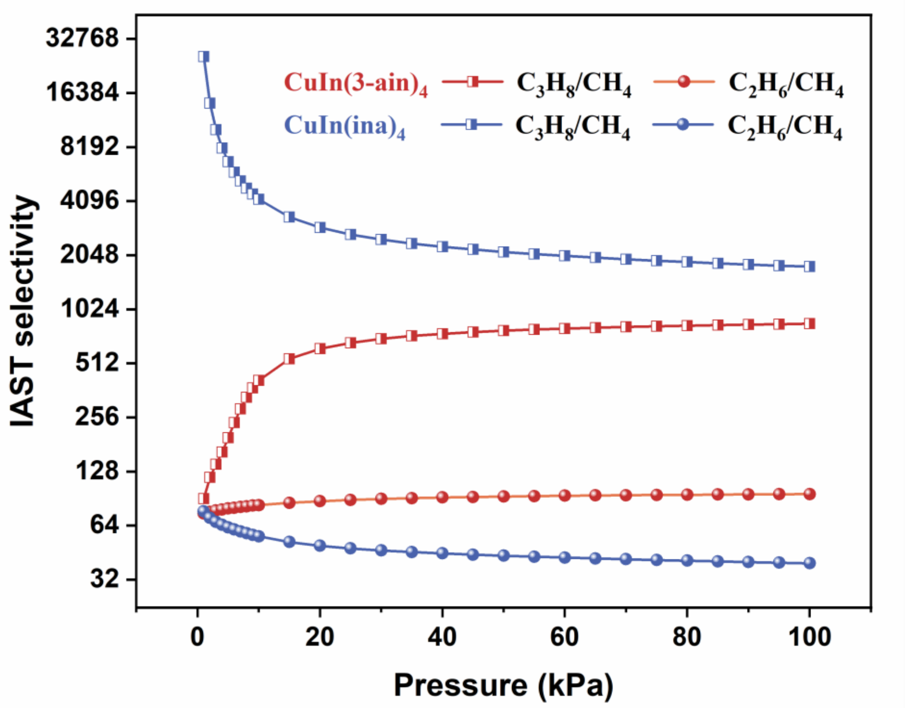

Figure S14. IAST selectivity of CuIn(ina)$_4$ and CuIn(3-ain)$_4$ towards C_3H_8/CH_4 (1:99) and C_2H_6/CH_4 (1:99) at 298 K.

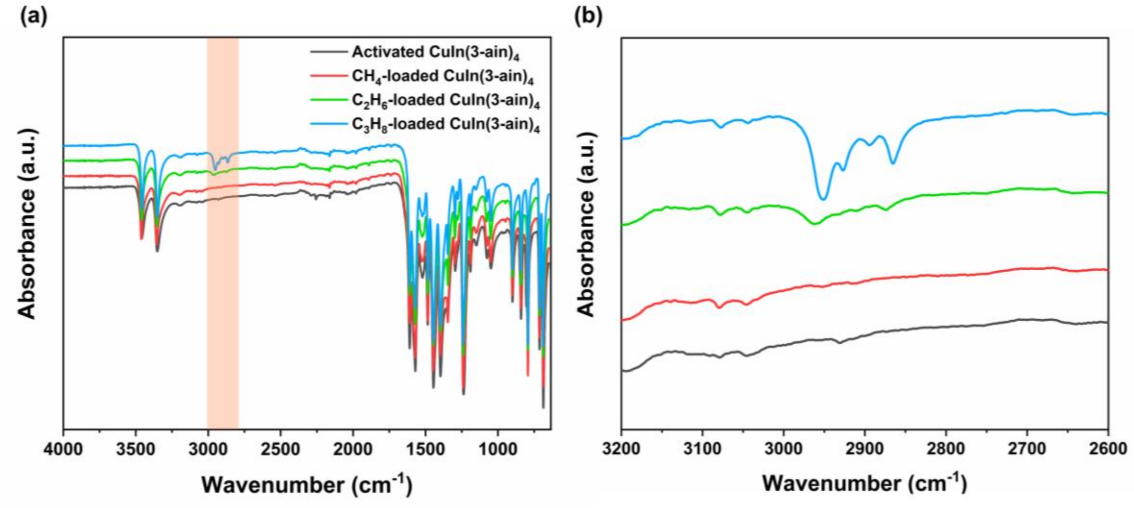

Figure S15. (a) FT-IR spectra of activated, CH_4, C_2H_6 and C_3H_8-loaded CuIn(3-ain)$_4$; (b) The partial magnification of the FT-IR spectra.

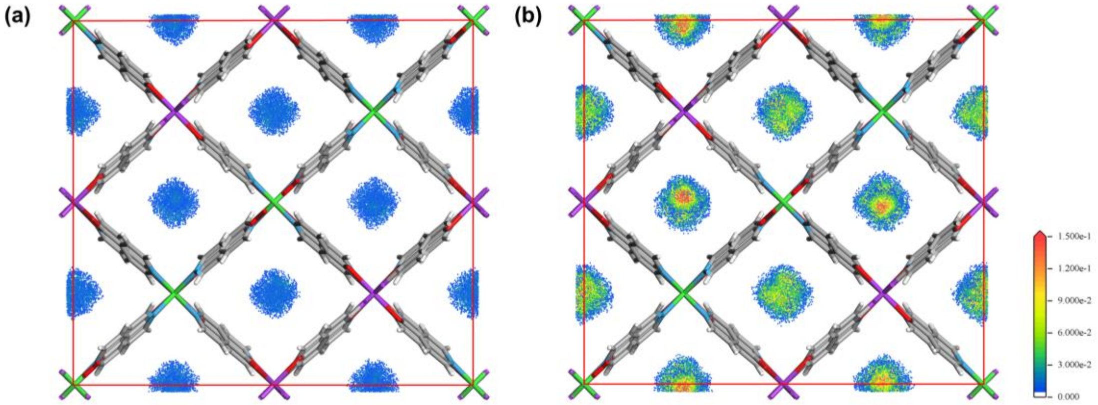

Figure S16. Density distribution of CH_4 on CuIn(ina)$_4$ at (a) 1 kPa, (b) 100 kPa and 298 K.

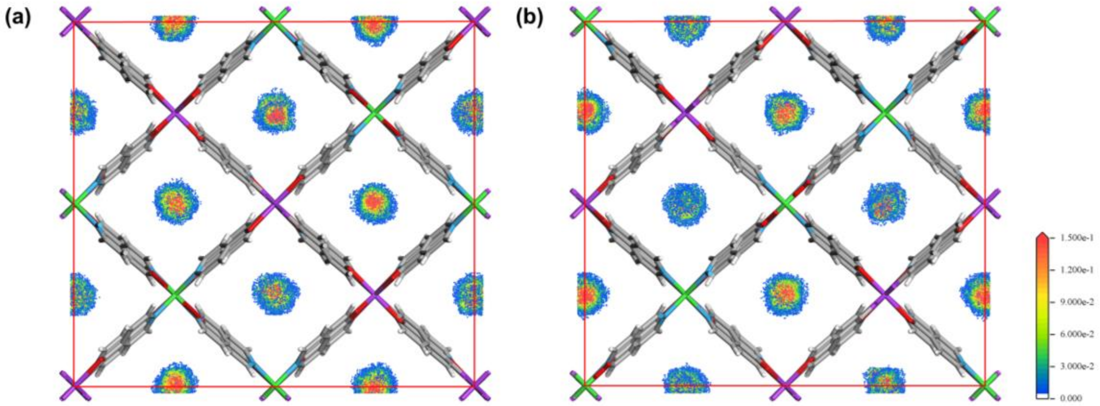

Figure S17. Density distribution of C_2H_6 on CuIn(ina)$_4$ at (a) 1 kPa, (b) 100 kPa and 298 K.

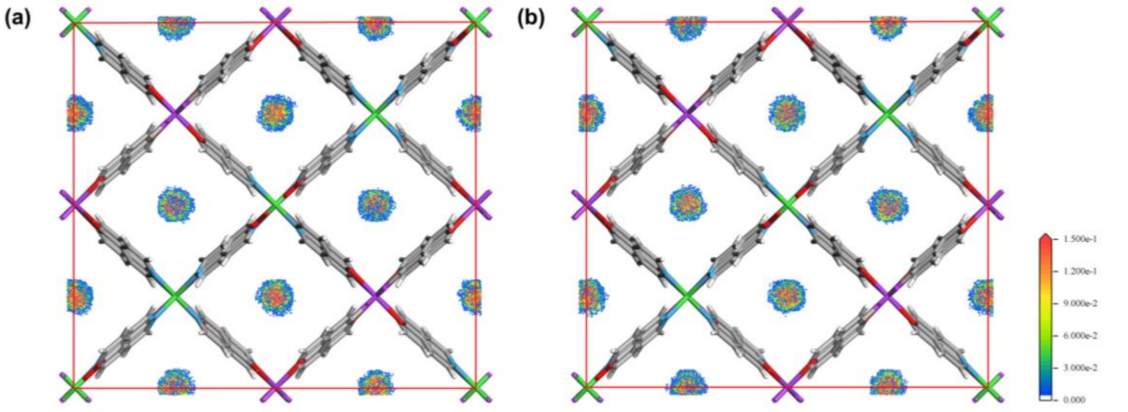

Figure S18. Density distribution of C_3H_8 on CuIn(ina)$_4$ at (a) 1 kPa, (b) 100 kPa and 298 K.

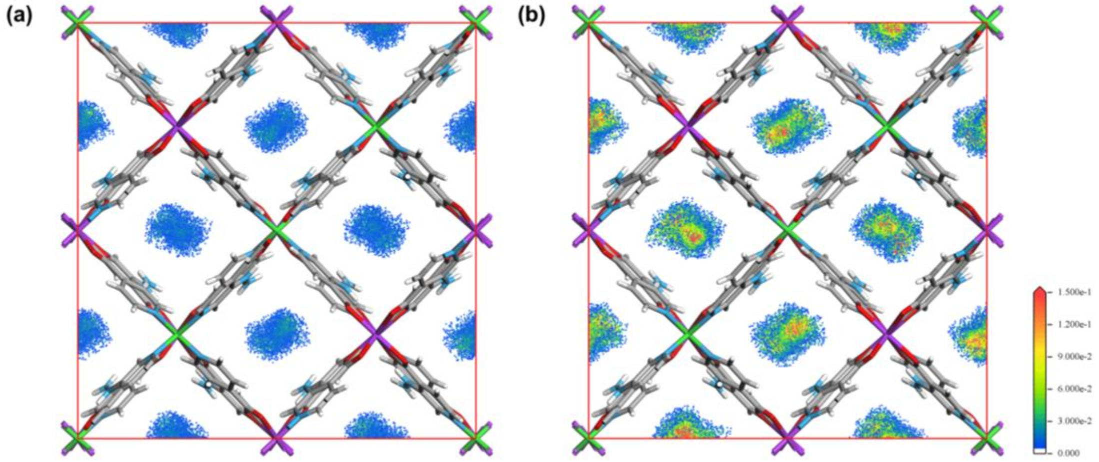

Figure S19. Density distribution of CH_4 on CuIn(3-ain)$_4$ at (a) 1 kPa, (b) 100 kPa and 298 K.

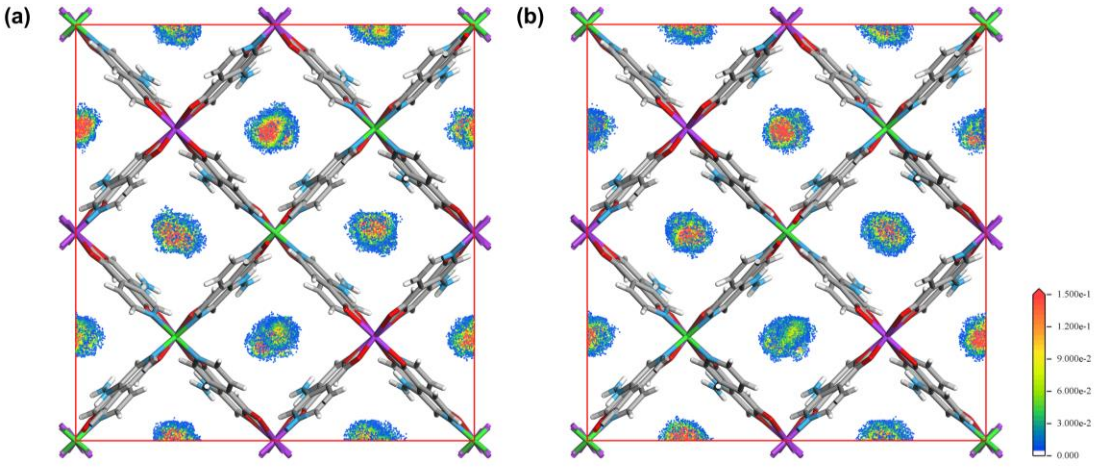

Figure S20. Density distribution of C_2H_6 on CuIn(3-ain)$_4$ at (a) 1 kPa, (b) 100 kPa and 298 K.

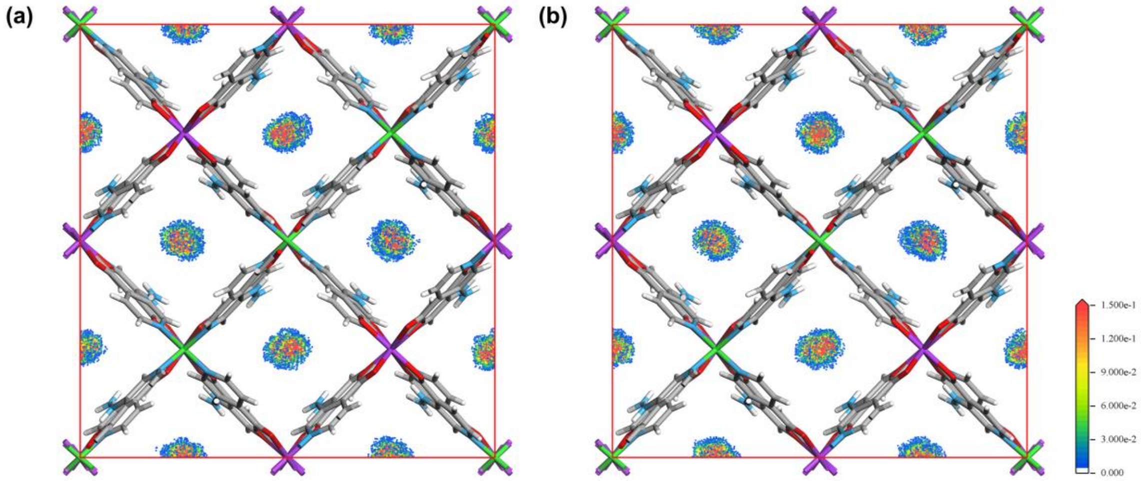

Figure S21. Density distribution of C_3H_8 on CuIn(3-ain)$_4$ at (a) 1 kPa, (b) 100 kPa and 298 K.

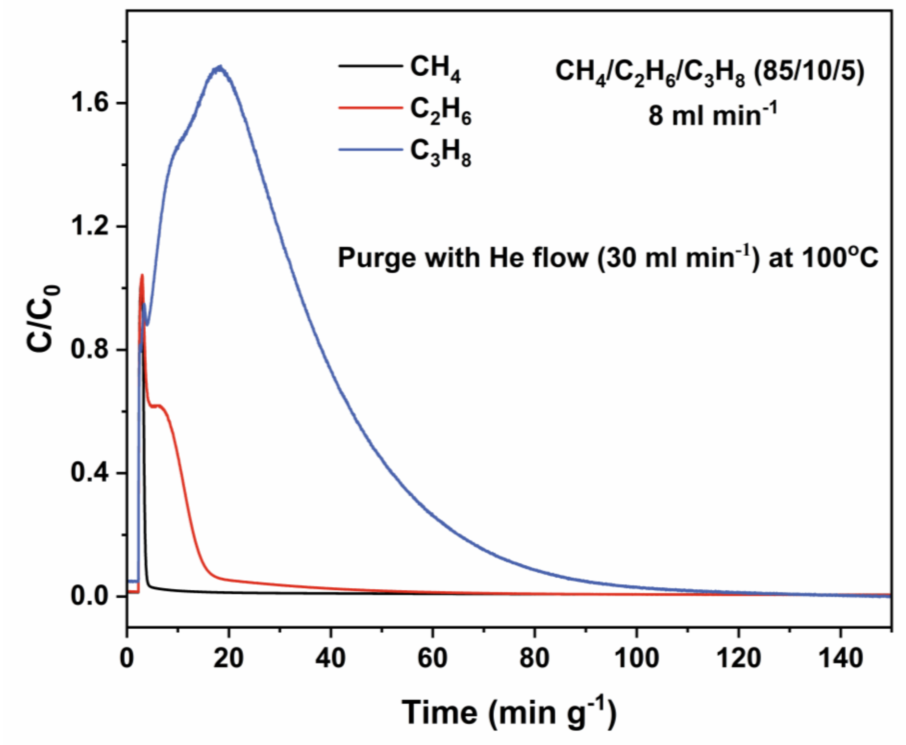

Figure S22. Desorption curves were recorded on the column at 100°C under He flow of 30 mL min^{-1}.

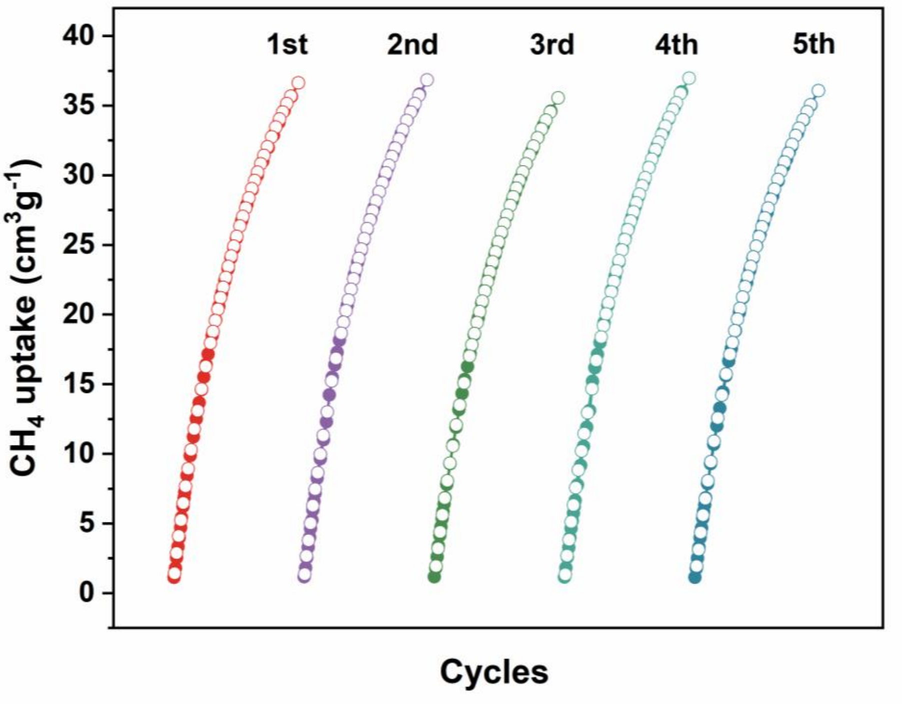

Figure S23. Cycling CH_4 adsorption-desorption experiments for CuIn(3-ain)$_4$.

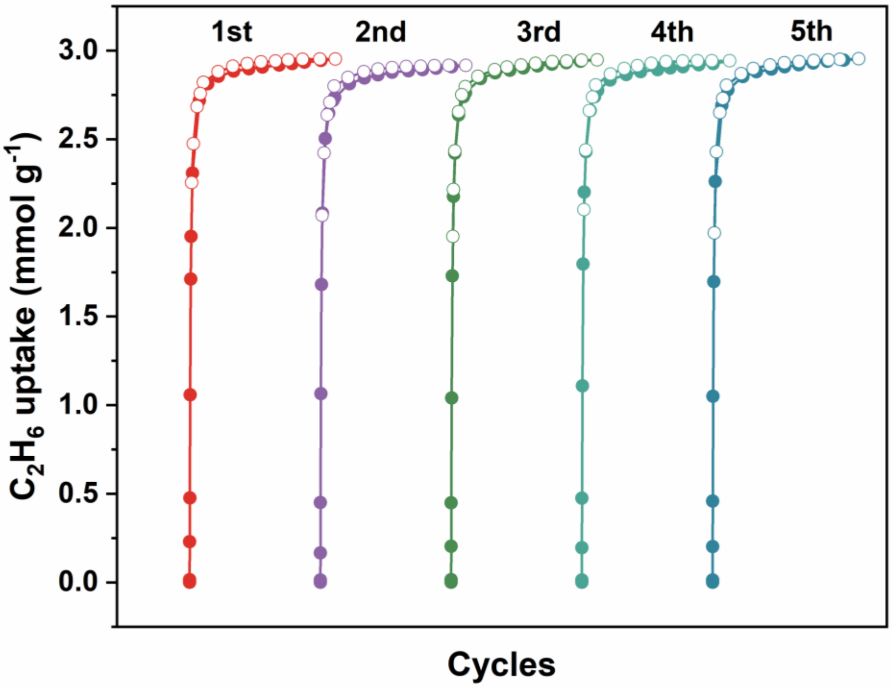

Figure S24. Cycling C_2H_6 adsorption-desorption experiments for CuIn(3-ain)$_4$.

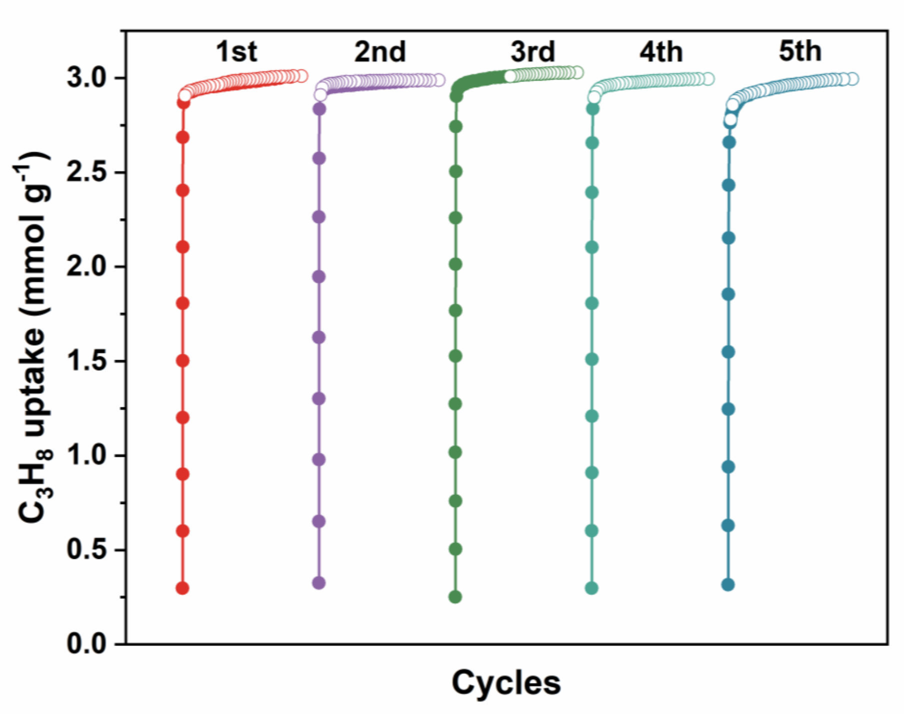

Figure S25. Cycling C_3H_8 adsorption-desorption experiments for CuIn(3-ain)$_4$.

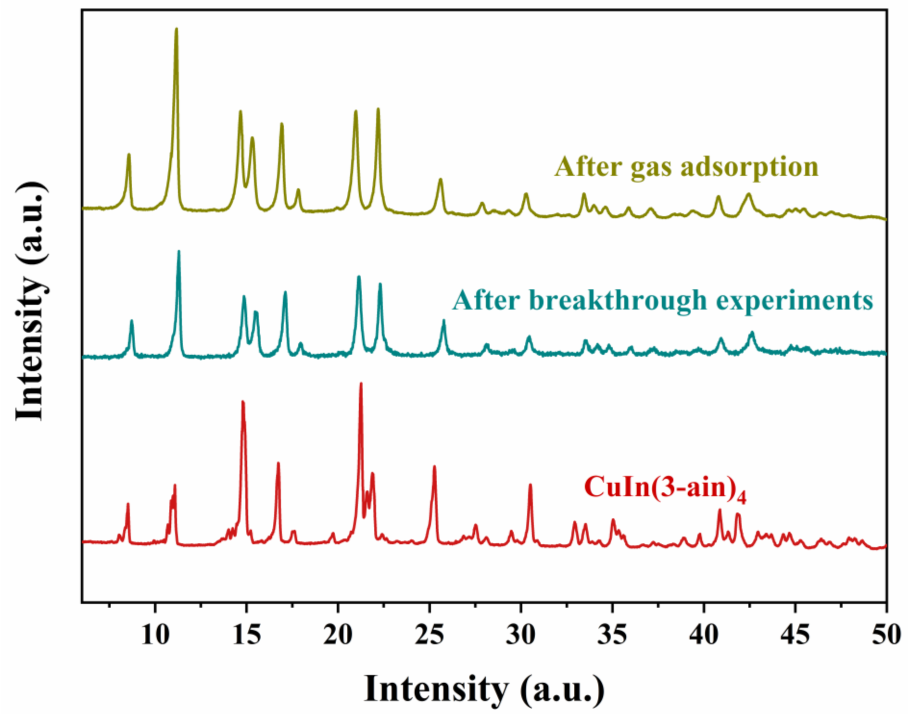

Figure S26. PXRD patterns of CuIn(3-ain)$_4$ after gas adsorption and breakthrough experiments.

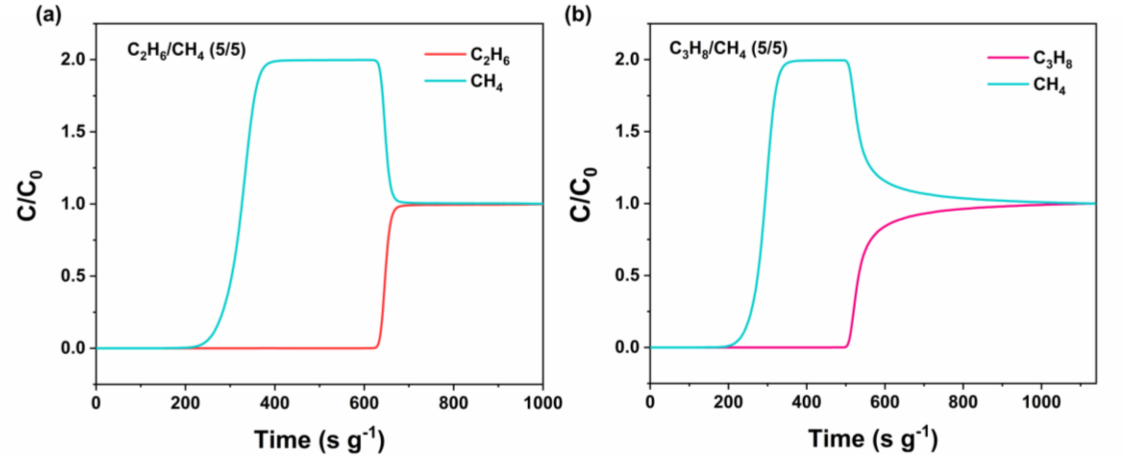

Figure S27. Dynamic breakthrough curves for (a) C_2H_6/CH_4 (5/5, v/v) and (b) C_3H_8/CH_4 (5/5, v/v) binary mixtures (total flow rate of 8 mL min^{-1}) at 298 K and 1.0 bar.

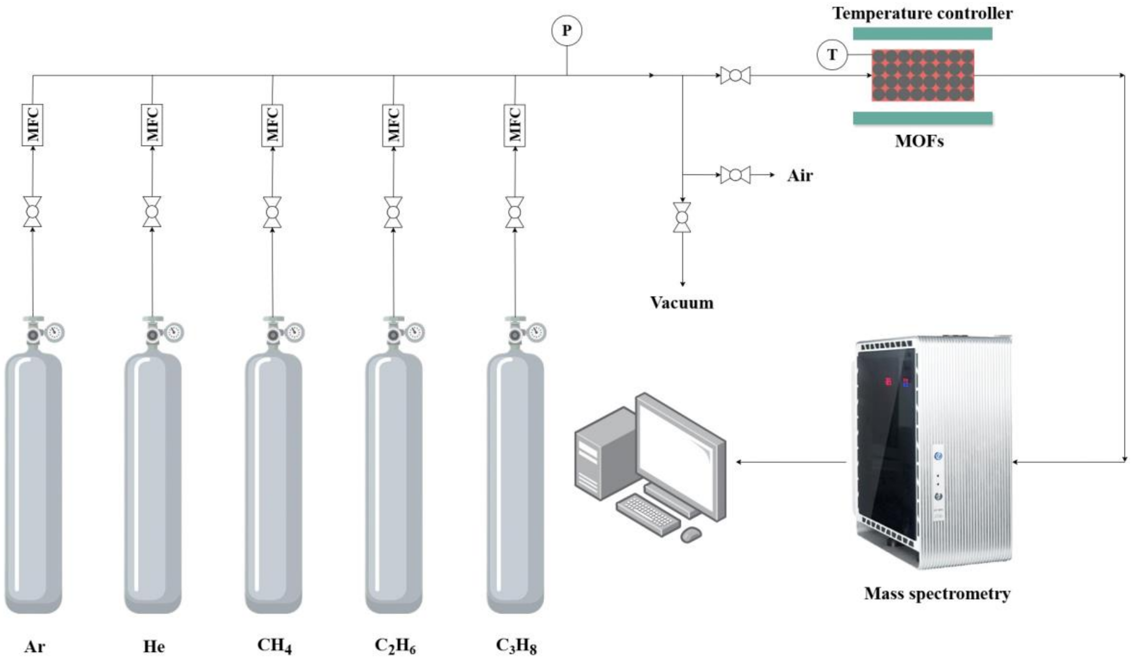

Figure S28. Schematic illustration of the setup for breakthrough experiments.

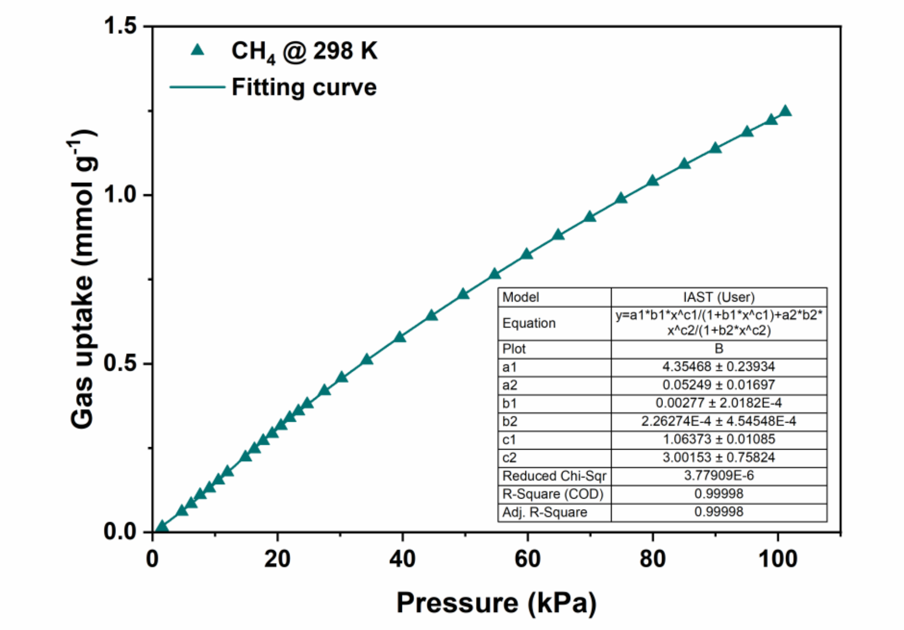

Model	IAST (User)
Equation	y=a1*b1*x^c1/(1+b1*x^c1)+a2*b2*x^c2/(1+b2*x^c2)
Plot	B
a1	4.35468 ± 0.23934
a2	0.05249 ± 0.01697
b1	0.00277 ± 2.0182E-4
b2	2.26274E-4 ± 4.54548E-4
c1	1.06373 ± 0.01085
c2	3.00153 ± 0.75824
Reduced Chi-Sqr	3.77909E-6
R-Square (COD)	0.99998
Adj. R-Square	0.99998

Figure S29. Dual-site Langmuir-Freundlich model for CH_4 adsorption isotherm on $CuIn(ina)_4$ at 298 K.

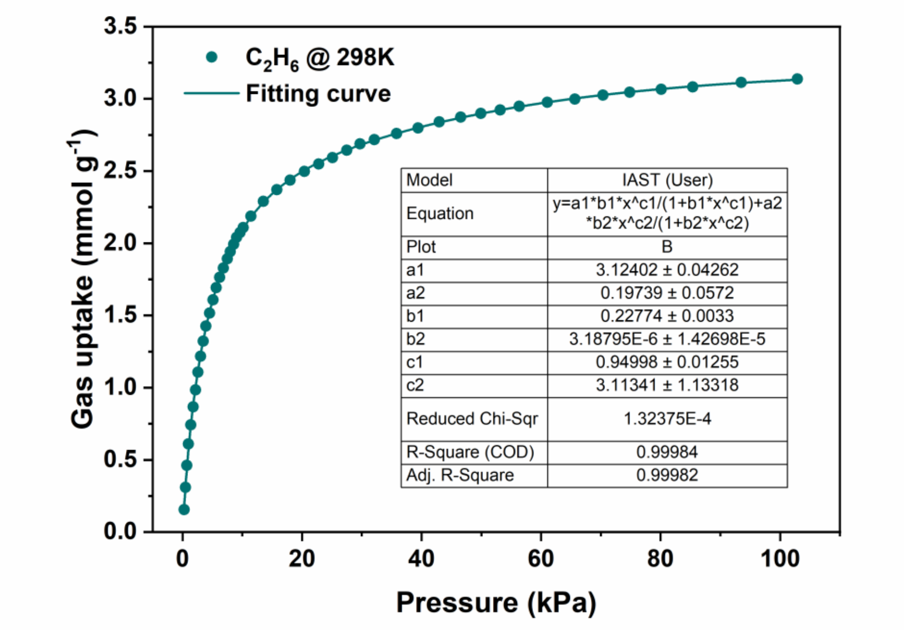

Model	IAST (User)
Equation	y=a1*b1*x^c1/(1+b1*x^c1)+a2 *b2*x^c2/(1+b2*x^c2)
Plot	B
a1	3.12402 ± 0.04262
a2	0.19739 ± 0.0572
b1	0.22774 ± 0.0033
b2	3.18795E-6 ± 1.42698E-5
c1	0.94998 ± 0.01255
c2	3.11341 ± 1.13318
Reduced Chi-Sqr	1.32375E-4
R-Square (COD)	0.99984
Adj. R-Square	0.99982

Figure S30. Dual-site Langmuir-Freundlich model for C_2H_6 adsorption isotherm on CuIn(ina)$_4$ at 298 K.

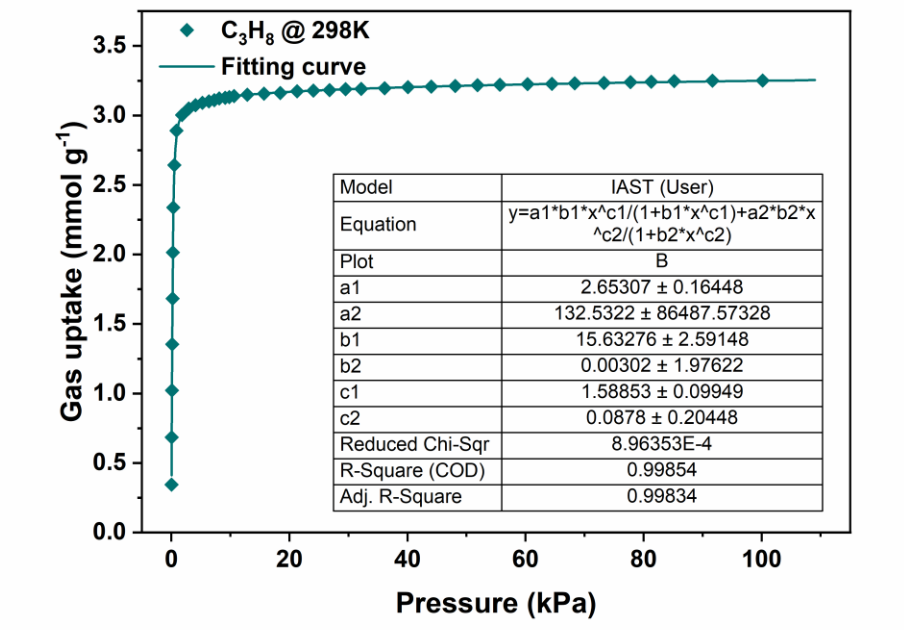

Model	IAST (User)
Equation	y=a1*b1*x^c1/(1+b1*x^c1)+a2*b2*x ^c2/(1+b2*x^c2)
Plot	B
a1	2.65307 ± 0.16448
a2	132.5322 ± 86487.57328
b1	15.63276 ± 2.59148
b2	0.00302 ± 1.97622
c1	1.58853 ± 0.09949
c2	0.0878 ± 0.20448
Reduced Chi-Sqr	8.96353E-4
R-Square (COD)	0.99854
Adj. R-Square	0.99834

Figure S31. Dual-site Langmuir-Freundlich model for C_3H_8 adsorption isotherm on CuIn(ina)$_4$ at 298 K.

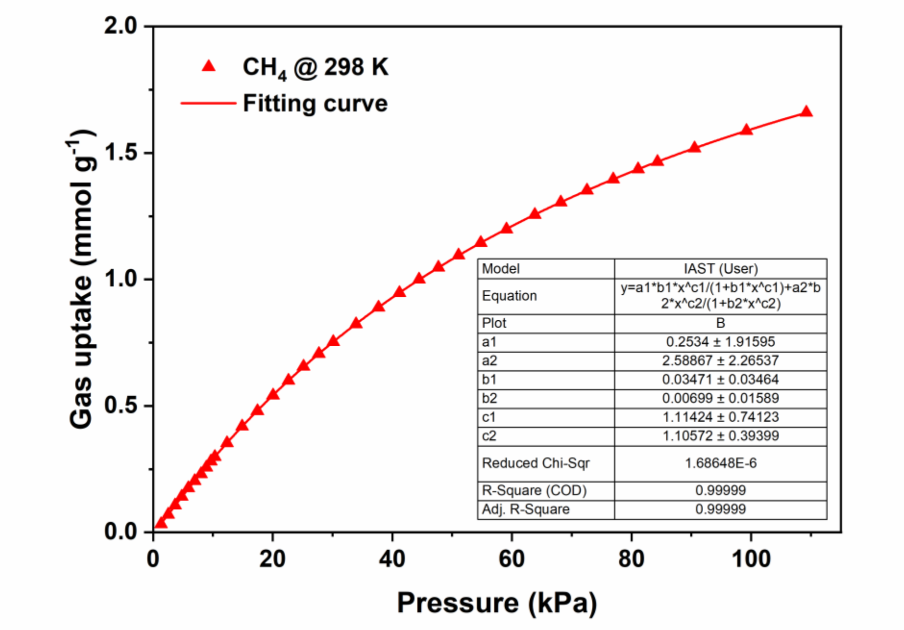

Figure S32. Dual-site Langmuir-Freundlich model for CH_4 adsorption isotherm on CuIn(3-ain)$_4$ at 298 K.

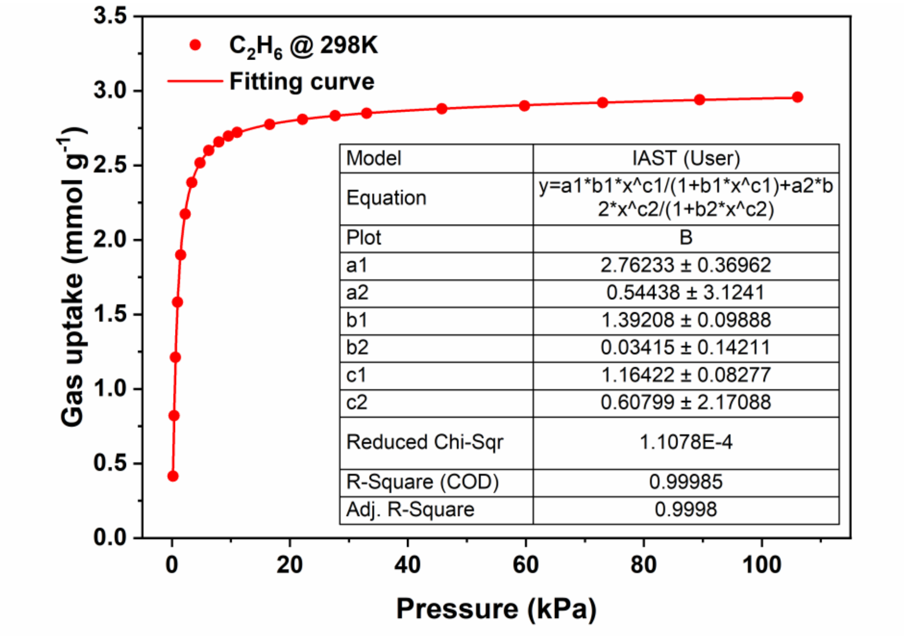

Model	IAST (User)
Equation	y=a1*b1*x^c1/(1+b1*x^c1)+a2*b2*x^c2/(1+b2*x^c2)
Plot	B
a1	2.76233 ± 0.36962
a2	0.54438 ± 3.1241
b1	1.39208 ± 0.09888
b2	0.03415 ± 0.14211
c1	1.16422 ± 0.08277
c2	0.60799 ± 2.17088
Reduced Chi-Sqr	1.1078E-4
R-Square (COD)	0.99985
Adj. R-Square	0.9998

Figure S33. Dual-site Langmuir-Freundlich model for C_2H_6 adsorption isotherm on CuIn(3-ain)$_4$ at 298 K.

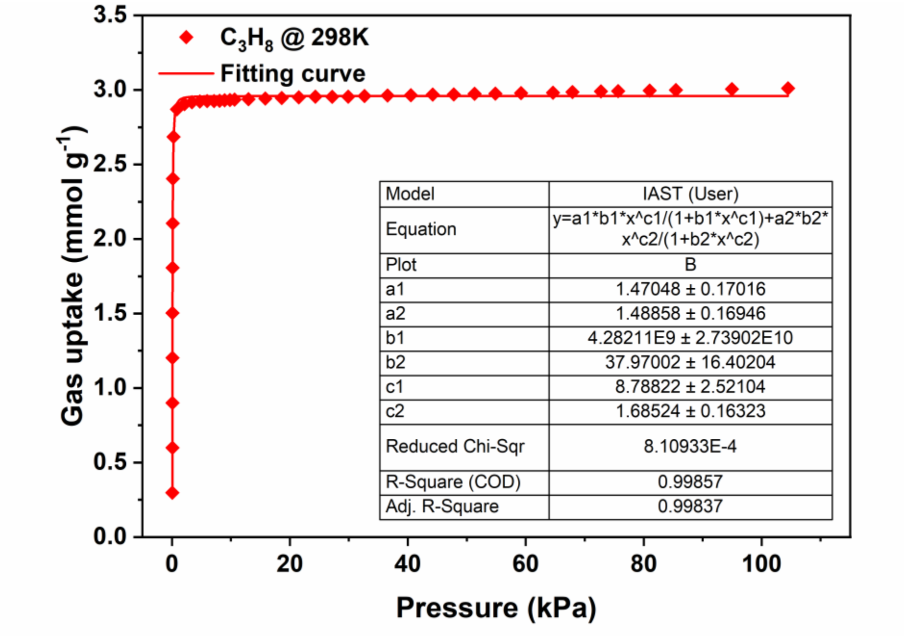

Model	IAST (User)
Equation	y=a1*b1*x^c1/(1+b1*x^c1)+a2*b2*x^c2/(1+b2*x^c2)
Plot	B
a1	1.47048 ± 0.17016
a2	1.48858 ± 0.16946
b1	4.28211E9 ± 2.73902E10
b2	37.97002 ± 16.40204
c1	8.78822 ± 2.52104
c2	1.68524 ± 0.16323
Reduced Chi-Sqr	8.10933E-4
R-Square (COD)	0.99857
Adj. R-Square	0.99837

Figure S34. Dual-site Langmuir-Freundlich model for C_3H_8 adsorption isotherm on CuIn(3-ain)$_4$ at 298 K.

Table S1. Comparison of physical parameters of CH_4, C_2H_6, and C_3H_8.

	Molecular weight (g mol^{-1})	**Kinetic diameter (Å)**	**Boiling points (K)**	**Polarizability (10^{-25} cm^3)**	**Dipole moment (10^{-18} esu cm)**	**Quadruple moment (10^{-26} esu cm^2)**
CH_4	16.04	3.758	111.66	25.93	0	0
C_2H_6	30.07	4.443	184.55	44.3-44.7	0	0.65
C_3H_8	44.10	4.3-5.118	231.02	62.9-63.7	0.084	—

Table S2. Structure parameters and the calculated results for gas occupancy.

Adsorbent	**Adsorbate**	**ρ (g cm^{-3})**	**V$_c$ (Å^3)**	**Q (mmol g^{-1})**	**Gas occupancy**
CuIn(ina)$_4$	CH_4	1.277	1734.7	1.25	1.67
	C_2H_6	1.277	1734.7	3.14	4.19
	C_3H_8	1.277	1734.7	3.25	4.34
CuIn(3-ain)$_4$	CH_4	1.576	1899.3	1.66	2.99
	C_2H_6	1.576	1899.3	2.96	5.34
	C_3H_8	1.576	1899.3	3.01	5.42

Table S3. Structure parameters and the calculated results for gas density.

Adsorbent	Adsorbate	M (g mol^{-1})	V$_p$ (ml g^{-1})	Q (mmol g^{-1})	Gas density (g ml^{-1})
CuIn(ina)$_4$	CH_4	16	0.22	1.25	0.09
	C_2H_6	30	0.22	3.14	0.43
	C_3H_8	44	0.22	3.25	0.65
CuIn(3-ain)$_4$	CH_4	16	0.20	1.66	0.13
	C_2H_6	30	0.20	2.96	0.44
	C_3H_8	44	0.20	3.01	0.66

Table S4. Comparison of C3/C2 adsorption capacity and C_2H_6/CH_4 (50/50) and C_3H_8/CH_4 (50/50) selectivities of some reported materials (298 K, 1 bar).

MOFs	**C_3H_8 Uptake^a (mmol g^{-1})**	**C_2H_6 Uptake^a (mmol g^{-1})**	**C_3H_8/CH_4 (50:50) Selectivity^b**	**C_2H_6/CH_4 (50:50) Selectivity^b**	**Ref**
$CuIn(3\text{-}ain)_4$	3.01	2.96	1047	101	This work
$CuIn(ina)_4$	3.25	3.14	625	24	This work
ZUL-C2	2.52	2.82	632	91	[5]
ZUL-C1	2.72	2.95	73	22	[5]
Co-MOF	2.65	2.62	290	26	[6]
$Ni(TMBDC)(DABCO)_{0.5}$	5.54	5.81	274	29	[7]
JLU-Liu15	3.88	3.47	461.5	27.8	[8]
BSF-2	2.21	1.52	681	25	[9]
BSF-1	2.03	1.64	353	23	[9]
JLU-Liu6	2.58	2.15	274.6	20.4	[10]
NKM-101	3.34	2.92	223.1	20.1	[11]
JLU-Liu40	7.32	4.64	845	21	[12]
Ni(HBTC)(bipy)	6.18	5.85	1857	27.5	[13]
LIFM-ZZ-1	4.06	2.80	485	16	[14]
MIL-142A	5.32	3.82	1300	13.7	[15]
JLU-Liu22	4.15	3.30	271.5	14.4	[16]

[a] IAST selectivity under the condition of equimolar binary mixtures at 298 K and 100 kPa.

[b] Gas adsorption uptake at 298 K and 100 kPa.

Table S5. Comparison of C_2H_6 and C_3H_8 uptake at low pressure and IAST selectivity towards gas mixtures of C_2H_6/CH_4 (10/85) and C_3H_8/CH_4 (5/85) selectivities of some reported materials (298 K, 1 bar).

MOFs	**C_3H_8 uptake at 5kPa (mmol g^{-1})**	**C_2H_6 uptake at 10 kPa (mmol g^{-1})**	**C_3H_8/CH_4 (5:85) Selectivity^a**	**C_2H_6/CH_4 (10:85) Selectivity^a**	**Ref**
$CuIn(3\text{-ain})_4$	2.92	2.71	945	99	This work
$CuIn(ina)_4$	3.09	2.11	1164	32	This work
ZUL-C2	2.08	2.27	741	82	[5]
ZUL-C1	2.17	1.85	158	28	[5]
$Ni(TMBDC)(DABCO)_{0.5}$	3.37	2.93	274	29	[7]
BSF-2	1.13	0.62	681	25	[9]
NKM-101	1.85	1.82	189.66	18.19	[11]
JLU-Liu40	2.14	0.76	170.36	16.96	[12]
Ni(HBTC)(bipy)	4.52	1.5	317.5	16.9	[13]
JLU-Liu22	2.12	1.00	144.89	5.5	[16]
MOF-303	3.38	1.82	5114	26	[17]
SNNU-Bai69	1.33	0.66	214.4	25.3	[18]
TIFSIX-Cu-TPA	2.33	1.01	—	—	[19]
CMOM-7	2.71	1.14	151.4	17.1	[20]
0.3Gly@HKUST-1	4.13	1.10	—	—	[21]

^{a} IAST selectivity under the condition of equimolar binary mixtures at 298 K and 100 kPa.

References

1. L. Yang, Q. Gao, Y. M. Zhang, R. H. Wang and L. Z. Chen, Efficient C_2H_6/C_2H_4 adsorption separation by a microporous heterometal-organic framework, *J. Colloid Interf Sci.*, 2023, ***652***, 1093-1098.
2. L. P. Zhang, G. W. Guan, Y. T. Li, H. R. Liu, S. T. Zheng, Y. Jiang, R. Bai and Q. Y. Yang, Amino-Functionalized Metal-Organic Frameworks Featuring Ultra-Strong Ethane Nano-Traps for Efficient C_2H_6/C_2H_4 Separation, *Small*, 2024, e2402382.
3. A. K. Rappe, K. S. Colwell and C. J. Casewit, Application of a Universal Force-Field to Metal-Complexes, *Inorg. Chem.*, 1993, ***32***, 3438-3450.
4. B. Delley, From molecules to solids with the DMol^3 approach, *J Chem Phys.*, 2000, ***113***, 7756-7764.
5. J. Y. Zhou, T. Ke, F. Steinke, N. Stock, Z. G. Zhang, Z. B. Bao, X. He, Q. L. Ren and Q. W. Yang, Tunable Confined Aliphatic Pore Environment in Robust Metal-Organic Frameworks for Efficient Separation of Gases with a Similar Structure, *J. Am. Chem. Soc.*, 2022, ***144***, 14322-14329.
6. L. Lan, N. Lu, J. C. Yin, Q. Gao, F. F. Lang, Y. H. Zhang, H. X. Nie, N. Li and X. H. Bu, Simultaneous extraction of C_3H_8 and C_2H_6 from ternary $C_3H_8/C_2H_6/CH_4$ mixtures in an ultra-microporous metal-organic framework, *Chem. Eng. J.*, *2023,* ***476,*** 146750.
7. Y. F. Wu, Z. W. Liu, J. J. Peng, X. Wang, X. Zhou and Z. Li, Enhancing Selective Adsorption in a Robust Pillared-Layer Metal-Organic Framework via Channel Methylation for the Recovery of C2-C3 from Natural Gas, *ACS. Appl. Mater. Interfaces*, 2020, ***12***, 51499-51505.
8. X. L. Luo, L. B. Sun, J. Zhao, D. S. Li, D. M. Wang, G. H. Li, Q. S. Huo and Y. L. Liu, Three Metal-Organic Frameworks Based on Binodal Inorganic Building Units and Hetero-O, N Donor Ligand: Solvothermal Syntheses, Structures, and Gas Sorption Properties, *Cryst. Growth Des.*, 2015, ***15***, 4901-4907.
9. Y. B. Zhang, L. F. Yang, L. Y. Wang, X. L. Cui and H. B. Xing, Pillar iodination in functional boron cage hybrid supramolecular frameworks for high performance separation of light hydrocarbons, *J. Mater. Chem. A.*, 2019, ***7***, 27560-27566.
10. D. M. Wang, T. T. Zhao, Y. Cao, S. Yao, G. H. Li, Q. S. Huo and Y. L. Liu, High performance gas adsorption and separation of natural gas in two microporous metal-organic frameworks with ternary building units, *Chem. Commun.*, 2014, ***50***, 8648-8650.
11. Y. Qiao, X. Chang, J. Y. Zheng, M. Yi, Z. Chang, M. H. Yu and X. H. Bu, Self-Interpenetrated Water-Stable Microporous Metal-Organic Framework toward Storage and Purification of Light Hydrocarbons, *Inorg. Chem.*, 2021, ***60***, 2749-2755.
12. Q. S. Sun, S. Yao, B. Liu, X. Y. Liu, G. H. Li, X. Y. Liu and Y. L. Liu, A novel polyhedron-based metal-organic framework with high performance for gas uptake and light hydrocarbon separation, *Dalton T.*, 2018, ***47***, 5005-5010.
13. P. T. Guo, M. Chang, T. G. Yan, Y. X. Li and D. H. Liu, A pillared-layer metal-organic framework for efficient separation of $C_3H_8/C_2H_6/CH_4$ in natural gas, *Chin. J. Chem. Eng.*, 2022, ***42***, 10-16.
14. Z. Zeng, W. Wang, X. H. Xiong, N. X. Zhu, Y. Y. Xiong, Z. W. Wei and J. J. Jiang, Flexible Microporous Copper(II) Metal-Organic Framework toward the Storage and Separation of C1-C3 Hydrocarbons in Natural Gas, *Inorg. Chem.*, 2021, ***60***, 8456-8460.
15. Y. N. Yuan, H. X. Wu, Y. Z. Xu, D. F. Lv, S. Tu, Y. Wu, Z. Li and Q. B. Xia, Selective extraction of methane from C1/C2/C3 on moisture-resistant MIL-142A with interpenetrated networks, *Chem. Eng. J.*, 2020, ***395***, 125057.

16. D. M. Wang, B. Liu, S. Yao, T. Wang, G. H. Li, Q. S. Huo and Y. L. Liu, A polyhedral metal-organic framework based on the supermolecular building block strategy exhibiting high performance for carbon dioxide capture and separation of light hydrocarbons, *Chem. Commun.*, 2015, ***51***, 15287-15289.
17. S. K. Xian, J. J. Peng, H. Pandey, T. Thonhauser, H. Wang and J. Li, Robust Metal-Organic Frameworks with High Industrial Applicability in Efficient Recovery of C_3H_8 and C_2H_6 from Natural Gas Upgrading, *Engineering-Prc*, 2023, ***23***, 56-63.
18. M. Ding, Q. Wang, H. T. Cheng and J. F. Bai, Synthesis, structure and highly selective C_3H_8/CH_4 and C_2H_6/CH_4 adsorption of a (4,8)-c ternary flu-metal-organic framework based upon both $[Sc_4O_2(COO)_8]$ and $[Cu_4OCl_6]$ clusters, *Crystengcomm*, 2022, ***24***, 2388-2392.
19. Y. X. Chen, Y. J. Jiang, J. H. Li, X. H. Hong, H. F. Ni, L. Y. Wang, N. Ma, M. M. Tong, R. Krishna and Y. B. Zhang, Optimizing the cask effect in multicomponent natural gas purification to provide high methane productivity, *AIChE J.*, 2024, ***70***, e18320.
20. C. H. Deng, L. Zhao, M. Y. Gao, S. Darwish, B. Q. Song, D. Sensharma, M. Lusi, Y. L. Peng, S. Mukherjee and M. J. Zaworotko, Ultramicroporous Lonsdaleite Topology MOF with High Propane Uptake and Propane/Methane Selectivity for Propane Capture from Simulated Natural Gas, *ACS Mater. Lett.*, 2023, ***6***, 56-65.
21. Y. F. Wu, Y. W. Sun, J. Xiao, X. Wang and Z. Li, Glycine-Modified HKUST-1 with Simultaneously Enhanced Moisture Stability and Improved Adsorption for Light Hydrocarbons Separation, *ACS Sustainable Chem. Eng.*, 2019, *7,* 1557-1563.